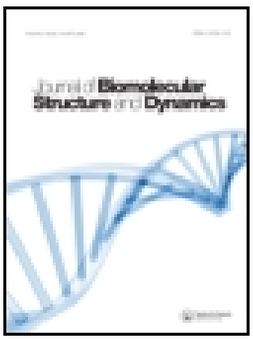

Taylor & Francis
Taylor & Francis Group

Journal of Biomolecular Structure and Dynamics

ISSN: 0739-1102 (Print) 1538-0254 (Online) Journal homepage: https://www.tandfonline.com/loi/tbsd20

The guanidiniocarbonylpyrrole - fluorophore conjugates as theragnostic tools for DPP III monitoring and inhibition

Mirsada Ćehić, Josipa Suć Sajko, Zrinka Karačić, Patryciusz Piotrowski, Tamara Šmidlehner, Ivanka Jerić, Carsten Schmuck, Ivo Piantanida & Sanja Tomić

To cite this article: Mirsada Ćehić, Josipa Suć Sajko, Zrinka Karačić, Patryciusz Piotrowski, Tamara Šmidlehner, Ivanka Jerić, Carsten Schmuck, Ivo Piantanida & Sanja Tomić (2019): The guanidiniocarbonylpyrrole - fluorophore conjugates as theragnostic tools for DPP III monitoring and inhibition, Journal of Biomolecular Structure and Dynamics, DOI: 10.1080/07391102.2019.1664936

To link to this article: https://doi.org/10.1080/07391102.2019.1664936

The guanidiniocarbonylpyrrole - fluorophore conjugates as theragnostic tools for DPP III monitoring and inhibition

Mirsada Ćehić[1], Josipa Sućˇ Sajko[1], Zrinka Karačić[1], Patryciusz Piotrowski[2], Tamara Šmidlehner[1], Ivanka Jerić[1], Carsten Schmuck[2], Ivo Piantanida[1]* and Sanja Tomić*

[1]Ruđer Bošković Institute, HR-10000 Zagreb, Croatia

[2]Institute of Organic Chemistry, University of Duisburg-Essen, 45117 Essen, Germany

*Corresponding authors Ivo Piantanida and Sanja Tomić

E-mails: pianta@irb.hr; sanja.tomic@irb.hr

Keywords: DPP III inhibitor • fluorescence • pyrene • cyanine • guanidiniocarbonyl-pyrrole

List of Abbreviations:

GCP	guanidiniocarbonylpyrrole
DPP III	dipeptidyl peptidase III
Arg_2-2NA	Arg-Arg-2-naphthylamide
MD	molecular dynamics

Abstract

Study of seven new guanidiniocarbonylpyrrole (GCP) - fluorophore conjugates interactions with dipeptidyl peptidase III (DPP III) showed that all compounds bind strongly ($K_s \approx \mu M$) to enzyme active site, but with very different fluorimetric response (varying from quenching to strong increase), dependent on the fluorophore type and intramolecular pre-organisation of molecule. Positively charged lysine side chain improved significantly compound solubility but diminished fluorescence increase upon DPP III binding and

completely abolished inhibitory effect on DPP III activity, whereas linker-neutral analogues showed stronger emission increase and were efficient enzyme inhibitors. By far the best fluorimetric response and inhibitive properties showed cyanine – GCP analogue, thus being promising lead compound for both, enzyme sensing and bio-activity inhibiting (theragnostic) studies of DPP III in the future.

Introduction

The zinc-dependent exopeptidase dipeptidyl peptidase III, a single member of the M49 enzyme family is broadly distributed in mammalian tissues and thought to contribute in the final steps of the normal intracellular protein catabolism. (Prajapati & Chauhan 2011), (Baršun, Jajčanin, Vukelić, Špoljarić & Abramić 2007). However, pronounced affinity for some bioactive peptides (angiotensins II, III, IV and opioid peptides) suggests more specific functions (Baršun et al. 2007; Dhanda, Singh, Singh & Singh 2008; Pang et al. 2016; Tomić, Kovacević & Tomić 2016). Also, there is an increasing amount of experimental evidence indicating involvement of DPP III in development of some cancers in human (Mačak Šafranko et al. 2015; Prajapati & Chauhan 2016). Because of that it is potential target for curing several pathophysiological conditions in human and recently, it has attracted attention of several research groups all over the world. Yet, the knowledge of its exact role in these processes is far from being satisfactory.

In order to advance the knowledge about human DPP III (hDPP III) we studied its enzyme mechanism and tested influence of the selected mutations as well as of flavonoids and newly synthesized inhibitors on the enzymatic activity (Agić et al. 2017; Matovina et al. 2017; Smidlehner, Karacic, Tomić, Schmuck & Piantanida 2018). The present research is the continuation of the earlier one about influence of guanidiniocarbonyl-pyrrole analogues on hDPP III.

In further design of potential DPP III enzyme inhibitors, we have chosen as the start point the structure of the standard DPP III substrate, Arg-Arg-2-naphthylamide (Arg_2-2NA), changing the basic Arg-Arg guanidines ($pK_a \approx 11$) by slightly acidic guanidiniocarbonyl ($pK_a \approx 6$) and naphthylamide by pyrene fluorophore, taking care to sterically protect peptide bond against enzyme cleavage by carboxy-group: such guanidiniocarbonyl-pyrrole analogue (Scheme 1: **PE1**) showing promising enzyme inhibition properties (Matić et al. 2016).

The general structure of guanidiniocarbonyl-pyrrole moiety (GCP) (Schmuck 2011) looked like a good alternative to Arg-Arg- moiety with the possible advantage of lower pK_a value.

Namely, guanidiniocarbonyl-pyrrole moiety with $pK_a \approx 6$ is neutral at physiological conditions (pH 7.4) and could form strong H-bonds within the enzyme binding site, as well as strong hydrophobic interactions.

One of the extensively used polarity-sensitive probes is pyrene: its fluorescence has been intensively applied for the characterisation of micro-heterogeneous systems (Winnik 1993; Lehrer 1997; Lakowicz 1999). The long lifetime of the pyrene excited state and the ability of pyrene to form excimer with significantly altered emission properties allow versatile applications of pyrene for probing of nucleic acid structures, both as a single pyrene label (Yamana et al. 2001; Korshun, Stetsenko & Gait 2002), or in excimer-forming pairs or as multi-pyrene probes (Kostenko et al. 2001; Mahara et al. 2002).

Another intriguing alternative for sensitive fluorimetric probes are cyanine dyes, intrinsically non-fluorescent due to the non-radiative excitation decay but showing exceptionally strong fluorescence when bound to the target, due to the blocked rotation around methine bond (Armitage 2005; Tatikolov 2012).

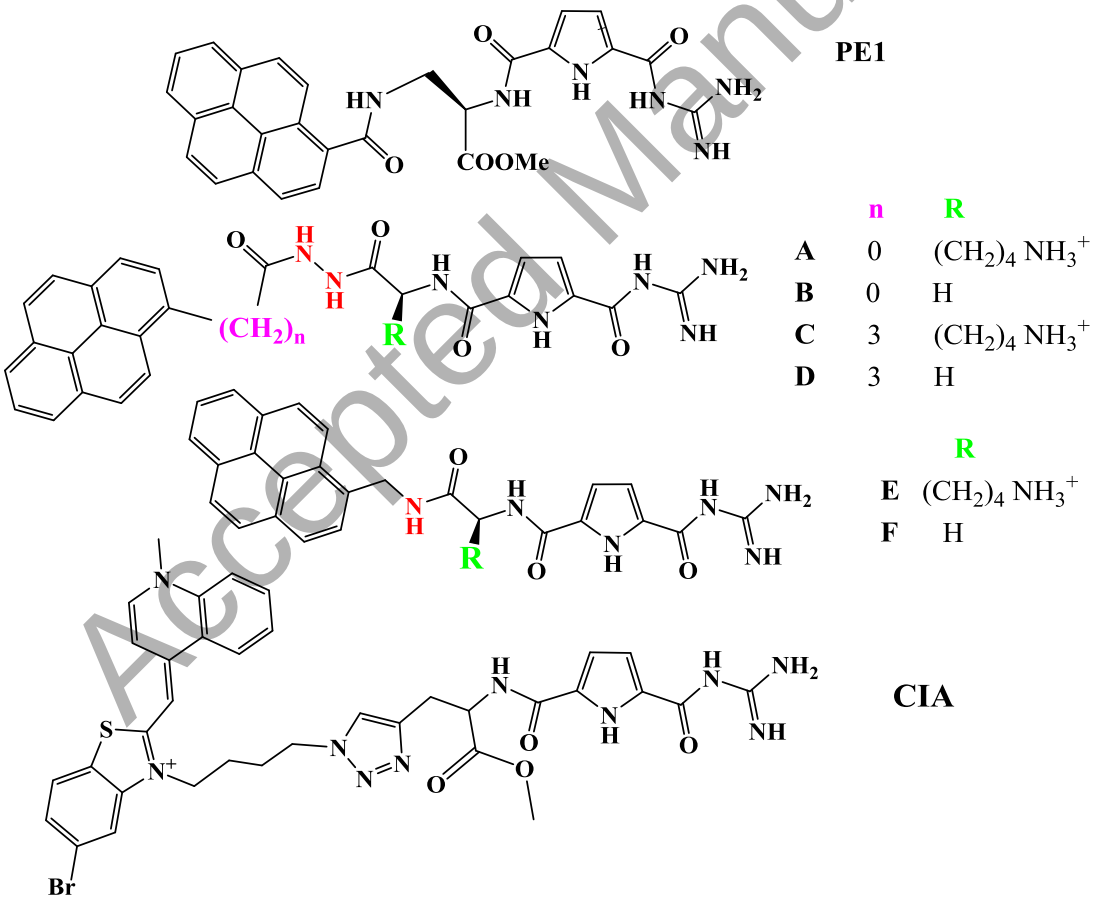

Scheme 1. Novel compounds **A-F** and **CIA** and previously studied DPP III inhibitor PE1 (Matić et al. 2016).

The guanidiniocarbonyl-pyrrole (GCP) – fluorophore conjugates can also be perceived as theragnostic tools (Shi, Wu & Pan 2016) since they are able to report presence of DPP III and inhibit it simultaneously. Moreover, such conjugates would report their displacement from enzyme binding site by any other small molecule (e.g. substrate), thus in situ monitoring situation at enzyme active site and availability for enzymatic reaction.

Inspired by promising results observed by **PE1** (Matić et al. 2016), we designed and prepared a new series of guanidiniocarbonyl-pyrrole (GCP) – fluorophore conjugates (Scheme 1), systematically varying:

a) the linker length (**A**, **B**, **C**, **D** being longer than **PE1,** and **E**, **F** of the same length);

b) linker rigidity (**E**, **F** being more flexible than **PE1** due to absence of COOMe and aliphatic link to pyrene) and by insertion of hydrazine moiety in **A**, **B**, **C**, **D** (thus rigidifying the linker structure);

c) by variation of the charge and steric properties in respect to insertion in DPP III binding site by the introduction of lysine

Last but not least, inspired by promising results of previously studied GCP-cyanine conjugate (Smidlehner et al. 2018), we prepared by similar procedure analogue (**CIA**, Scheme 1) with reversed connectivity of cyanine dye (here over benzothiazolium part) and also with extended linker, it's length comparable to **C**, **D**.

In this work, we combined synthetic organic chemistry, set of methods for study of thermodynamic equilibrium and kinetic enzyme / ligand properties and molecular dynamics simulations to study novel ligand / human DPP III interactions. Particularly, the fluorimetric response of novel compounds upon interaction with DPP III was in detail studied since fluorescence-based techniques are by far the most intensively used methods in biomedical and biological studies (Mycek & Pogue 2003; Lakowicz 1999). The aim of the study was to prepare novel enzyme inhibitors and/or substrates, able to report on inhibition/enzymatic reaction by highly sensitive fluorimetric response.

Results and Discussion

Synthesis:

Seven new compounds (Scheme 1, **A**-**F** and **CIA**) were prepared by standard synthetic procedures in rather different synthetic routes, particularly for pyrene analogues **A**-**F** depending on the reactivity of available precursors. Due to the diversity of approaches, all

synthetic details are given in Supp. Info., while structural characterization of final compounds is in the Experimental section.

Characterization of new compounds in aqueous medium:

A, C, **E** and **CIA** were moderately soluble in redistilled water (c=1×10^{-3} M), and **B, D** and **F** were dissolved in dimethyl sulfoxide (c=1×10^{-3} M). Stock solutions were diluted with buffer sodium cacodylate (pH 7.0 or pH 7.4, I = 0.05 M).

The absorbancies of buffered solutions of studied compounds (Figure 1) were proportional to their concentrations up to c=2×10^{-6} M (molar extinction coefficients, ε, in Supp. Info., Table S1). Buffered solutions of studied compounds (c ≈ 2×10^{-5} M, pH 7.0, I = 0.05 M, t=25 °C) were stable for a day, some of them subsequently starting to precipitate. Therefore, for all further measurements every day fresh solutions were prepared.

The UV/Vis spectra of **A**, **C, E** and **F** didn't change significantly upon the temperature increase up to 95^{o}C and reproducibility of UV/Vis spectra upon cooling back to 25^{o}C was excellent (Supp. Info., Figure S2). All mentioned is indicating that the studied compounds **A**, **C, E** and **F** do not aggregate by intermolecular or intramolecular interactions at experimental conditions used. At variance to **A**, **C, E** and **F**; compounds **B** and **D** showed pronounced changes in their UV/Vis spectra of upon heating (Supp. Info., Figure S2), indicating intermolecular or intramolecular aromatic interactions. Upon cooling UV/Vis spectrum of **B** was almost restored, suggesting reversibility of aromatic interactions, while UV/Vis spectrum of **D** revealed a substantial increase of spectrum and baseline, attributed to formation of opalescent colloid.

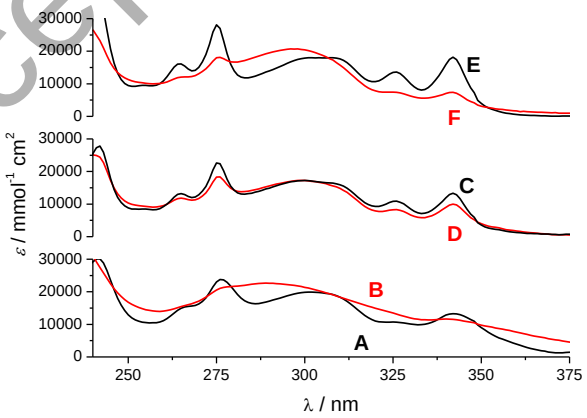

Figure 1. UV/vis spectra of **A-F** at pH 7.0, sodium cacodylate buffer, I = 0.05 M: positively charged **Lys**-derivatives (black lines: **A**, **C**, **E**) are s and neutral **Gly**-analogues (red lines: **B**, **D**, **F**).

Fluorescence emission of pyrene derivatives **A-F** was proportional to their concentrations up to 1×10^{-6} M, suggesting no intermolecular interactions and thus no aggregation of compounds. The spectra at $c = 2\times10^{-7}$ M (Figure 2) demonstrate differences in fluorescence emission as a direct consequence of a compound structure.

Derivatives **A**, **B** show emission typical for pyrene-1-carbonyl derivatives, whereby emission of **B** is strongly quenched in respect to **A**. The **C-F** fluorescence spectra correspond to pyrene-1-aliphatic derivatives. However, in **C-F** series there are distinct differences in emission spectra shape, namely **D** and **F** showing sharp vibronic bands at 378, 396 and 420 nm typical for free-motional pyrene, whereas spectra of their analogues (**C** and **E**) were strongly quenched and broadened. In addition, **E** emission almost completely lost the vibronic structure of three pyrene maxima. Such differences in emission concur with pronounced temperature-induced changes in UV/vis spectra of **B**, **C**, **E** (but not **A**, **F**, **D**) and strongly support for **B**, **C** and **E** involvement of pyrene in the intramolecular aromatic stacking interactions with pyrrole (Yamana et al. 2001; Korshun et al. 2002). This difference in emission and UV/vis spectral properties can be attributed to the lysine in **A**, **F**, **D**, sterically and by positive charge hydratation hampering self-folding of a molecule.

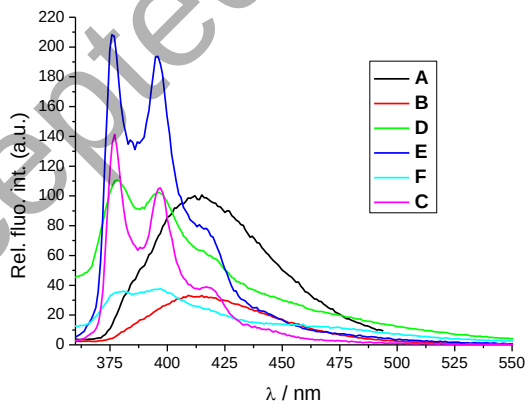

Figure 2. Fluorescence spectra of **A-F** at $c = 2\times10^{-7}$ M at various instrument setup (slits), thus only **A-B**; **C-D** and **E-F** pairs can be mutually compared. Done at pH 7.0, sodium cacodylate buffer, I = 0.05 M.

Cyanine analogue **CIA** was non-fluorescent in the aqueous solutions due to the well-known non-radiative excitation decay by rotation around the methine bond (Armitage 2005).

*Interactions of **A-F, CIA** with hDPP III:*

Further, we determined the non-covalent interactions of all studied compounds with the hDPP III inactive E451A mutant (to prevent eventual peptide bond cleavage), by fluorimetric titration experiments (Figure 3). Intriguingly, pyrene-derivatives response to E451 binding was strongly dependent on a compound structure. The pyrene-1-carbonyl analogues **A** and **B** emission was quenched by E451A, whereby lysine analogue **A** yielded significantly stronger response. That was in agreement with **A** intramolecularly non-folded conformation, whereas intramolecular emission quenching of **B** didn't leave the possibility of significant further quenching by E451A.

Pyrene-1-aliphatic derivatives **C**-**F** responded to E451 by emission enhancement, whereby much stronger increase was observed for neutral analogues **D** and **F** in comparison to positively charged lysine analogues **C** and **E**. Since **D** and **F** intrinsic emission is, due to the self-folding, quenched in respect to **C** and **E** (Figure 2), it seems that binding to E451A induced their unfolding and stretching, whereby GCP unit is immersed deep into enzyme binding site and very long linker allow pyrene to stay far from any aromatic stacking interaction and emit correspondingly stronger fluorescence.

The cyanine analogue **CIA**, intrinsically non-fluorescent, responded by strong emission upon binding to E451A (Supp. Info, Fig. S3), clearly indicating that free rotation of cyanine chromophore around methine bond is significantly hampered by the binding event.

Processing of the titration data by non-linear fitting to dye / E451A 1:1 stoichiometry (Supp. Info., Fig. S3) gave excellent correlation (r=0.999) and binding constants for complexes formed (Table 1). Almost all studied compounds showed similar micromolar affinity toward hDPP III E451A mutant, which defines them as efficient ligands at biorelevant conditions.

Intriguingly, **CIA** affinity toward hDPP III E451A mutant was 30 times stronger in comparison to previously studied close analogue (Smidlehner et al. 2018), which could be attributed to the reversed connectivity of a cyanine to the aliphatic linker.

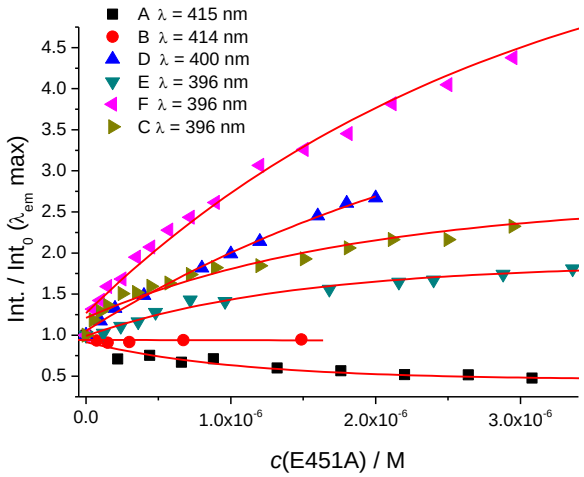

Figure 3. Fluorimetric titration of pyrene analogues **A-F** (c = 1×10^{-8} M, λ_{exc} ≈ 340 nm) with E451A, at pH 7.0, I=0.05 M, sodium cacodylate buffer. Normalized with respect to starting Int_0 at compound emission λ_{max} (396 - 420 nm).

Table 1. Binding constants ([a]logK_s) and fluorescence change ([b]Int/Int_0) of **A-F, CIA** with E451A, calculated by processing fluorimetric titrations (c(dye)=1×10^{-8} M), at pH 7, sodium cacodylate buffer, I = 0.05 M.

A	B	C	D	E	F	CIA
6.3	c	6.4	6.4	6.1	6.5	6.5
0.5	[C]0.95	3.3	10	1.7	6.7	d

[a] Processing of the titration data by non-linear fitting to dye / E451 1:1 stoichiometry.

[b] Int_0 – starting fluorescence intensity of dye; Int – fluorescence intensity of dye/ E451A complex calculated by the non-linear fitting.

[c] Too small change hampered accurate processing of titration data. Note that emission quenching is **RED** (**A**, **B**), and emission increase **BLUE** (**C-F, CIA**).

[d] Int_0 = 0.

Kinetic studies with wt-hDPP III:

Since all compounds possess peptide bonds, they could be potential hDPP III substrates or, failing peptide bond cleavage, potent inhibitors. For that reason we checked their influence

on the hDPP III catalysed hydrolysis of the synthetic substrate Arg_2-2NA. All compounds were stable at experimental conditions, thus we further fluorimetrically monitored the reaction of human wt-DPP III with an artificial substrate Arg_2-2NA, detecting the release of the product, 2-naphthylamine (λ_{ex} = 332 nm and λ_{em} = 420 nm) (Abramić et al. 2004; Kumar et al. 2016). It should be noted that the experimental conditions of this assay partially overlap with emission of pyrene (λ_{ex} = 342 nm and λ_{em} = 400-420 nm). However, in control experiments the pyrene fluorescence of compounds **A-F** didn't change, thus any emission change during enzymatic reaction with the substrate (Arg_2-2NA) could be attributed to the proportional increase of Arg_2-2NA decomposition product: 2-naphthylamine formation.

The measurements were performed at 25°C and in 20 mM Tris-HCl buffer pH 7.4 (Abramić et al. 2004; Kumar et al. 2016), and analysis of kinetic parameters by nonlinear regression analysis of data using GraphPad Prism 5 software (GraphPad) revealed that only **D**, **F** and **CIA** showed significant effect on the enzymatic reaction (Figure 4).

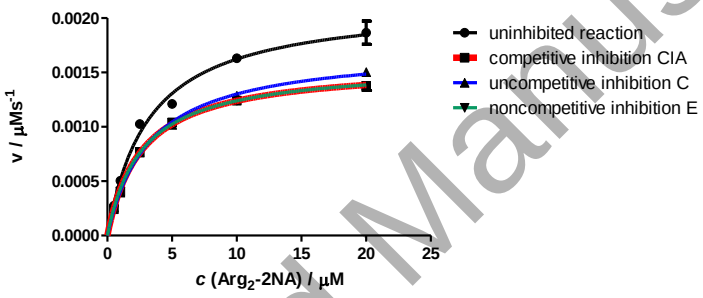

Figure 4. Michaelis Menten kinetics reaction profile of uninhibited reaction of human DPP III (20 pM); with the Arg2-2NA substrate (varied 1 µM - 200 µM; **black line**) and with the addition of inhibitors **D** (0.1 µM; **blue**), **F** (0.1 µM; **green**) and **CIA** (0.1 µM; **red**) (0.2 µM), in 20 mM Tris-HCl buffer pH 7.4. Note that green and red line overlap. A graphical representation of measurement results obtained by programme GraphPad (GraphPad).

Detailed analysis (Tables 2 and S2 and Figures S4-S11) revealed following order in efficiency of the hDPP3 enzyme inhibition: **CIA** (K_i=228 ± 53 nM) > **D** (K_i=295 ± 35 nM) > **F** (K_i=335 ± 32 nM) are somewhat better than previously reported cyanine analogue efficiency (K_i 370 nM) (Smidlehner et al. 2018). However, novel compounds are still not as effective DPP3 inhibitors as peptide tynorphin (K_i=70 nM) (Yamamoto, Hashimoto, Shimamura, Yamaguchi & Hazato 2000).

Table 2. Experimentally obtained kinetic parameters for hDPP3 III (wt) hydrolysis of Arg_2-2NA in buffered solution (Tris HCl, pH = 7.4, *I*=20 mM) with compounds **D**, **F** and **CIA**

Compound	Type of inhibition	K_i/nM	K_m/μM	k_{cat}/s^{-1}
D	uncompetitive	295 ± 35	3.3 ± 0.1	17.3 ± 0.2
F	noncompetitive	335 ± 32	2.7 ± 0.1	15.7 ± 0.2
CIA	competitive	228 ± 53	5.2 ± 0.6	22.6 ± 0.1

Further on, structure – activity analysis revealed that all here presented efficient inhibitors (**D**, **F**, **CIA**) as well as previously studied **PE1** (Matić et al. 2016) and **Cy-GCP** (Smidlehner et al. 2018), lack the long positively charged side chain (in compounds **A**, **C**, **E** this is Lys), which seems to completely abolish inhibitive properties. Intriguingly, analogue **B** (hydrazine extended analogue of **PE1** (Matić et al. 2016)) didn't inhibit the enzymatic reaction, whereas its elongated and more flexible analogue **D** acted as a quite efficient inhibitor.

Molecular modelling studies:

As an aid to the understanding the influence of the compounds **F** and **CIA** on the hDPP III activity, their complexes were modelled and simulated in water solution. On the other hand, complexes of the hDPP III inactive mutant E451A, with compounds **A**, **D** and **E**, **F** and CIA were studied computational in order to get an insight into their mutual (intermolecular) interactions and to rationalize their binding affinities (Supp. Info., Table S3).

The complexes were obtained using the program AutoDock 4.2.6, wherein the complexes with the highest score (altogether 10 complexes were generated for each compound) and the binding mode similar to that of the natural substrates were selected for the further simulations. AutoDock 4.2.6 program has been mostly used to predict the ligand binding modes. Its scoring function (combining certain advantages of knowledge-based potentials and empirical scoring functions) was shown to be quite reliable; however, it ignores dynamical effects. So, in order to evaluate dynamical stability of the DPP III – ligand complexes and their mutual interactions we performed molecular dynamics (MD) simulations. Further on, the MMPBSA energies were calculated on a set of conformers sampled during MD simulation in water and the obtained values were considered as an approximation of the binding free energies.

For each pyrene containing compound, two to three initial structures were considered, while for **CIA** we selected four structures generated by AutoDock for further molecular dynamics (MD) simulations. **CIA – DPP III complex**

Four different binding modes of CIA to hDPP III were considered (Supp. Info., Figure S12). Binding of the ligand into the wild type enzyme and E451A mutant do not differ significantly (Supp. Info., Figure S13). According to the results of 100 ns MD simulations analysis the largest fluctuation of both protein and ligand experienced complexes with the ligand in the binding mode 2 (M2) (Supp. Info., Figures S14 and S15), while those with **CIA** in the binding mode 3 (M3) were the most stable, Supp. Info., Figures S14, S15 and 16. This is in line with their relative MMPBSA energies (Table SMM1). Namely, the MMPBSA energies (calculated on a set of conformers sampled during MD simulation in water), which can be considered as an approximation of the binding free energies, are for CIA bound in the binding mode 3 lower than the energies calculated for the DPP III - CIA complexes with the ligand bound in the first two modes. In all cases, the ligand binds close to the lower domain β sheet and remained close to its initial position during 100 ns of MD simulations. The ligand in the binding mode 3 only slightly changed the cyanine orientation while the conformation of the ligands in the other binding modes changed to somewhat larger extent during simulations. In order to test stability of the E451A−**CIA**-M3 complex in more details, we extended the MD simulations for another 100 ns. The structure obtained after 200 ns of MD simulations closely resembles the structures after the first 100 ns, i.e. we could conclude that the complex E451A − **CIA**-M3 is stable (Figure 5). With guanidiniocarbonylpyrrole (GCP) part **CIA** interacts with the amino acid residues that stabilize substrate (Glu316, Tyr318, Ala388, Asn391), while with COOMe it interacts with His568 and Glu598, the amino acid residues that actively participate in the hDPP III catalysed peptide hydrolysis reaction (Tomić et al. 2016). With Phe109 CIA Additionally, it also electrostatically interact with Glu451 during MD simulations of the complex with the wild type enzyme as shown in Figure 6. Apparently, by its binding to hDPP III **CIA** hinder proper accommodation of the preferred hDPP III substrate Arg_2-2NA into the enzyme active site and chemical reaction.

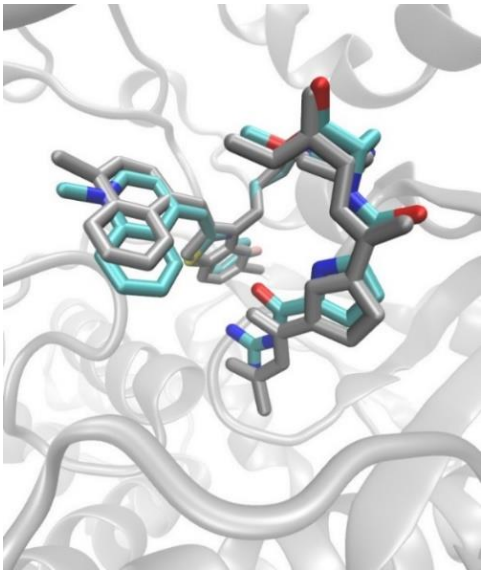

Figure 5. Overlay of the E451A – **CIA**-M3 complexes after 100 ns (gray) and 200 ns (cyan).

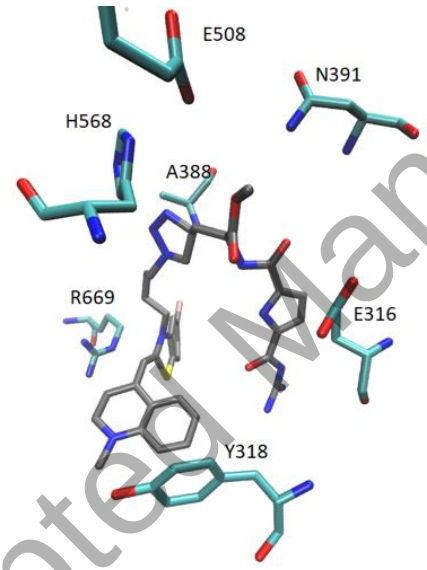

Figure 6. Interactions of **CIA**-M3 with the hDPP III active site amino acid residues. The structure obtained after 200 ns of MD simulations of the E451A – **CIA**-M3 complex.

A, **D, E** and **F / DPP III complexes**

Three different orientations of **F** in the wild type enzyme were simulated. The binding modes M1 and M2 induced significant changes of the protein compactness resulting with the RMSD > 3 Å (Supp. Info., Figure S17), while the RMSD for the protein in the complex with **F**-M3 was mostly below 2 Å. Since, the conformation and position of the ligand in this binding mode as well as intermolecular protein – ligand interactions were preserved during MD simulations, we assume that it represents a possible binding mode of **F**. Namely, RMSD was

used as an indicator that the convergence of the structure to a local minimum is achieved. Similarly to **CIA**, **F** also established strong electrostatic interaction with both Glu451 and His568 during MD simulations with the wild type enzyme as shown in Figure 7, and such binding is in accordance with its inhibitory behaviour. Differently from its position in the wild type enzyme, in the inactive mutant **F** remained close the lower domain during MD simulations (Supp. Info., Figure S18). Also, it should be noted that H – Pi interaction between Ala355 and pyrene is present in the DPP III – **F** complex during MD simulations (Supp. Info., Figure S19).

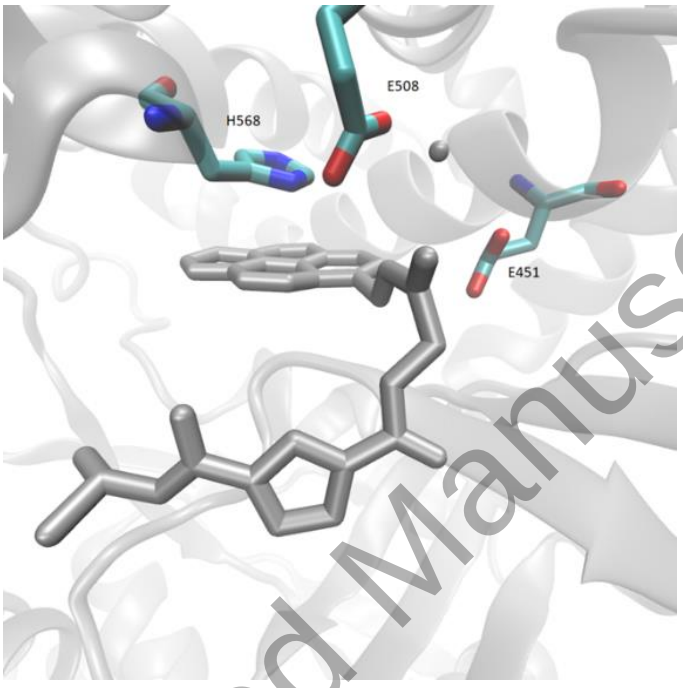

Figure 7. The amino acid residues from the hDPP III active site that interact with **F**-M2 (gray sticks) are shown in stick representation. The structure obtained after 100 ns of MD simulations of the hDPP III – E-M2 complex

Compounds **A**, **D** and **E** were simulated in the complex with the mutated enzyme, E451A; two different binding modes of **A** and **E** and there of **D** (Supp. Info., Table S3 and Figures S20-S22). Comparison of the most stable binding modes of these compounds revealed that they are of similar stability and do not induce the large conformational changes of the protein. The guanidine group makes strong hydrogen bond with the electrostatically negative lower domain patch comprising Glu329 Glu327 and Glu316, while the positively charged Lys from **A** and **E** interacts electrostatically (and occasionally by strong H-bonds) with Glu316 and Asp396, respectively. (Supp. Info., Table S4) during MD simulations. However, while **D** and **E** preferably bind close to the upper part of the lower domain β sheet and interact with

His568 and the other active site residues (Figure 8), **A** is firmly anchored close to the interdomain cleft entrance and it interacts with the distant part of the lower domain, except the pyrene ring which is stabilized by the upper domain residues and has the face to edge interaction with Phe556 (Figure 9). With the positively charged Lys it interacts with Glu316. Thus, the computational study suggests that **A** binds to hDPP III with similar affinity as the other compounds, but differently from them does not interfere with the Arg2-2NA hydrolysis.

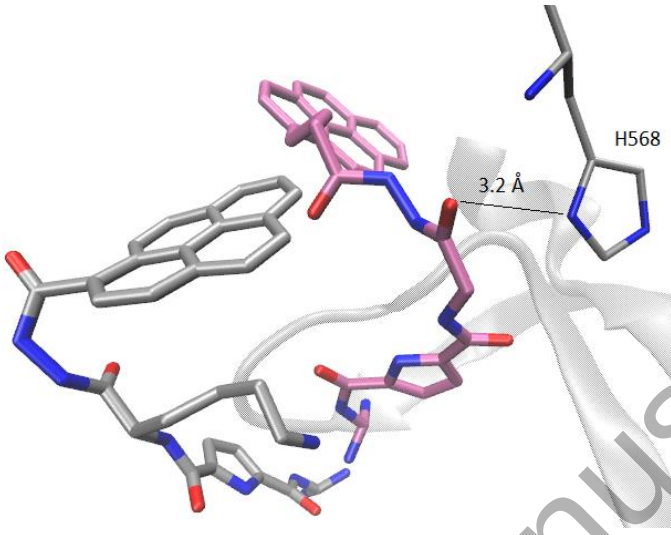

Figure 8. Overlay of the compounds **A** (gray), and **D** (mauve) in their preferable binding modes after 100 ns of MD simulation of their complexes with E451A. The zinc ion is shown as gray sphere, and the lower domain β sheet is shown in transparent ribbon representation.

.

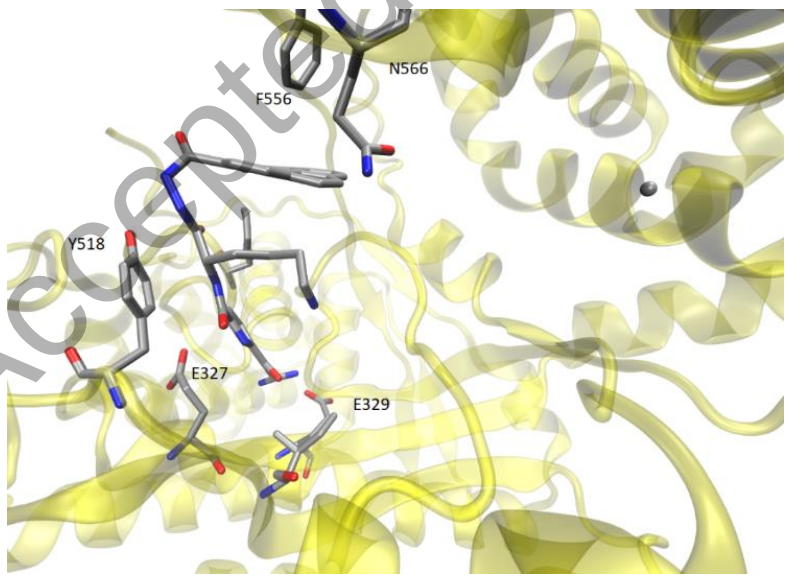

Figure 9. Interactions of **A**-M2 with protein. The structure obtained after 100 ns of MD simulations of the E451A – **A**-M2 complex.

Conclusions

A series of seven novel guanidiniocarbonylpyrrole (GCP) - fluorophore conjugates was prepared with the aim to study in detail the structural impacts of the linker length and rigidity, variation of the net positive charge and steric properties, as well as the type of the fluorophore (pyrene *vs* cyanine) on the non-covalent affinity toward DPP III, fluorimetric response and inhibitive properties of DPP III enzymatic reaction.

The fluorimetric emission of pyrene derivatives was by itself highly sensitive on a compound structure, neutral Gly-derivatives **B**, **D**, **F** showing strongly quenched emission due to self-folding, at variance to non-folded **A**, **C**, **E** positively charged Lys-analogues. Consequently, the fluorimetric response of various pyrene-derivatives upon binding to DPP III strongly varied: from emission increase (much stronger for Lys-analogues **C**, **E**) to the emission quenching (only pyrene-1-carbonyl, again stronger for Lys-analogues **A**). Cyanine analogue **CIA** showed strong emission only upon DPP III binding. Intriguingly, the binding affinity of all studied compounds was within the same order of magnitude (logK_s 6).

The impact of novel compounds on the enzymatic activity of human DPP III was directly related to the long positive side-arm of lysine, which abolished any inhibitive property of the corresponding analogues (**A**, **C**, **E**).

The molecular dynamics simulations combined with MMPBSA calculations and the intermolecular interactions analysis showed that complexes of the inactive hDPP III mutant E451A with **A**, **D**, **E**, **F** and **CIA** are of similar stability in water solution (in line with similar experimental binding constants). MMPBSA is assumed to be more accurate than most of the scoring functions, and at variance to them, it takes into account dynamical effects of the ligand binding (Wang et al. 2019). The more detailed study performed for the most effective inhibitor **CIA** revealed that the complex between the wild type enzyme and **CIA** (M3) was more stable than the **CIA** complex with the mutated enzyme E451A. This finding was attributed to the **CIA** interaction with Glu451 and His568 residues of the wild type enzyme, whereby these residues actively participate in the enzymatic reaction. In this way binding of **CIA** hindered both the substrate (Arg_2-2NA) binding and the enzymatic reaction. Compound **F** behaved similarly to **CIA**, but **F** interaction with Glu451 is weaker than interaction of **CIA** during MD simulation, probably resulting in somewhat weaker inhibitive effect.

All obtained results point toward cyanine-GCP analogues as the most promising lead compounds for possible DPP III-related theragnostic applications, namely simultaneously

monitoring by the fluorimetric response the enzyme active site and inhibiting the enzymatic reaction.

Experimental Section

General procedures:

Reaction solvents and triethylamine were distilled before use. All other reagents were used as obtained from Sigma Aldrich and Alfa Aesar. Thin-layer chromatography was performed on Silica Gel 60 F254 plates (Merck; Darmstadt, Germany). Melting points were measured on Kofler hot-stage microscope and are uncorrected. NMR spectra were recorded on Bruker Avance 600 and 300 MHz spectrometers, operating at 150. 92 or 75.47 MHz for 13C and 600.13 or 300.13 MHz for 1H nuclei. TMS or DMSO-$_{d6}$ were used as an internal standard. FT-IR spectra of the samples in KBr pellets were recorded at resolution of 4 cm^{-1} on an ABB Bomem MB102 single-beam spectrometer and were obtained as KBr pellets. HRMS analysis was performed on MALDI-TOF mass spectrometer operating in reflectron mode. Mass spectra were acquired by accumulating three spectra after 400 laser shots per spectrum. Calibrant and analyte spectra were obtained in positive ion mode. Calibration type was internal with calibrants produced by matrix ionization (monomeric, dimeric and trimeric CHCA), with azithromycin and angiotensin II dissolved in α-cyano-4-hydroxycinnamic acid matrix in the mass range m/z 190.0499 to 749.5157 or 1046.5417. Accurately measured spectra were internally calibrated and elemental analysis was performed on Data Explorer v. 4.9 Software with mass accuracy better than 5 ppm. Samples were prepared by mixing 1 μL of analyte methanol solution with 5 μL of saturated (10 mg/mL) solution of α-cyano-4-hydroxycinnamic acid (α-CHCA) and internal calibrants (0.1 mg/mL) dissolved in 50 % acetonitrile/0.1 % TFA. The UV-Vis spectra were recorded on a Varian Cary 100 Bio spectrometer in quartz cuvettes (1 cm). Fluorescence spectra were recorded on Varian Cary Eclipse fluorimeter in quartz cuvettes (1 cm). Under the experimental conditions used (~ 10^{-6} M) the absorbance and fluorescence intensities of **A-F, CIA** were proportional to their concentrations.

In fluorimetric experiments, excitation wavelengths at λ_{max} ~ 340 nm (**A-F**) or λ_{max} ~ 505 nm (**CIA**) were used in order to avoid absorption of excitation light by protein. Fluorimetric titrations were performed by adding portions of compound solution into the solution of the

protein. After mixing protein with studied compounds it was observed in all cases that equilibrium was reached in less than 120 seconds and in the next one hour fluorescence spectra of complexes remained constant.

Purification of human DPP III

Recombinant human DPP III was obtained by heterologous expression in Escherichia coli and purification according to (Špoljarić et al. 2009).

DPP III activity assay

The enzymatic activity of wild-type human DPP III was determined by a standard assay at 37 °C with Arg_2-2NA as substrate, using the colorimetric method as previously described (Abramić et al. 2004; Kumar et al. 2016). The *c*(human DPP III) = 20 pM; the substrate concentration (Arg_2-2NA) was varied from 1 μM to 200 μM. Kinetic parameters were obtained by nonlinear regression analysis of data according to the Michaelis-Menten model using GraphPad Prism 5 software (GraphPad).

Structure characterisation of A-F, CIA (detailed syntheses given in Supp. Info.):

Compound A:

^{1}H NMR (600 MHz, DMSO) δ / ppm 12.61 (NH, guanidino, s, 1H), 12.19 (NH, s, 1H), 10.55 (NH, hyd, s, 1H), 10.45 (NH, hyd, s, 1H), 8.83 (NH, amide, d, *J* = 8.0 Hz, 1H), 8.79 – 8.70 (NH_2, guanidino, s, 2H), 8.69 (CH, PCA, d, *J* = 9.2 Hz, 1H), 8.54 (NH_2, guanidino, s, 2H), 8.37 - 8.14 (CH, PCA, m, 8H), 7.95 (NH_3^+, Lys, s, 3H), 7.64 (CH, guanidino, s, 1H), 6.98 (CH, guanidino, s, 1H), 4.71 - 4.67 (α, Lys, m, 1H), 2.83 (ε, Lys, s, 2H), 2.00 – 1.80 (β, Lys, m, 2H), 1.66 (δ, Lys, d, *J* = 6.3 Hz, 2H), 1.60 - 1.51 (γ, Lys, m, 2H).

^{13}C NMR (151 MHz, DMSO) δ / ppm 171.2 (CO), 168.0 (CO), 159.8 (CO), 158.9 (CO), 155.6 (CNH), 132.4, 131.9 (C, guanidino), 130.7, 130.2 (CH, guanidino), 129.7 (C, PCA), 128.6, 128.3, 128.2, 127.2 (CH, PCA), 126.7, 125.9, 125.8, 125.7, 125.3 (C, PCA), 124.7, 124.5, 123.7, 123.5, 115.8 (CH, PCA), 113.8 (C, PCA), 51.4 (α, Lys), 38.6 (ε, Lys), 31.7 (β, Lys), 26.6 (δ, Lys), 22.5 (γ, Lys).

HRMS (MALDI-TOF/TOF) *m/z* = calc. for $\mathbf{C_{30}H_{32}N_8O_4^{2+}}$: 567,2468 $[M-H]^+$; found 567,2451 $[M-H]^+$.

Compound B:

^{1}H NMR (600 MHz, DMSO) δ / ppm 12.51 (NH, guanidino, s, 1H), 12.11 (NH, s, 1H), 10.54 (NH, hyd, s, 1H), 10.36 (NH, hyd, s, 1H), 8.99 (NH, amide, t, *J* = 5.8 Hz, 1H), 8.69 (NH_2, guanidino, bs, 2H), 8.66 (CH, PCA, d, *J* = 9.2 Hz, 1H), 8.55 (NH_2, guanidino, bs, 2H), 8.37 – 8.12 (CH, PCA, m, 8H), 7.61 (CH, guanidino, s, 1H), 6.96 (CH, guanidino, s, 1H), 4.13 (α, Gly, d, *J* = 5.8 Hz, 2H).

^{13}C NMR (151 MHz, DMSO) δ / ppm 168.4 (CO), 168.0 (CO), 159.7 (CO), 159.5 (CO), 155.5 (CNH), 132.5, 131.9 (C, guanidino), 130.7, 130.2 (CH, guanidino), 129.7 (C, PCA), 128.6, 128.3, 128.2, 127.2 (CH, PCA), 126.7, 125.9, 125.8, 125.7, 125.4 (C, PCA), 124.6, 124.5, 123.7, 123.5, 115.9 (CH, PCA), 113.0 (C, PCA), 45.4 (α, Gly).

HRMS (MALDI-TOF/TOF) *m/z* = calc. for $\mathbf{C_{26}H_{22}N_7O_4^+}$: 496.1733 $[M]^+$; found 496.1731 $[M]^+$.

Compound C:

^{1}H NMR (300 MHz, MeOD) δ / ppm 8.46 – 7.95 (CH, PMA, m, 9H), 7.15 (CH, guanidino, d, J = 4.0 Hz, 1H), 6.91 (CH, guanidino, d, J = 4.0 Hz, 1H), 5.15 (CH_2, PMA, s, 2H), 4.10 (α, Gly, s, 2H).

^{13}C NMR (151 MHz, MeOD) δ / ppm 170.8 (CO), 160.9 (CO), 159.9 (CO), 155.8 (CNH), 131.3, 130.8, 129.8, 128.6, 127.5, 127.0, 126.9, 126.5, 125.7, 124.9, 124.8, 124.4, 122.5, 115.2, 114.7, 114.6, 114.3, 112.9, 111.9 (CH, PMA, guanidino), 41.1 (CH_2, PMA), 31.4 (α, Gly).

HRMS (MALDI-TOF/TOF) m/z = calc. for $\mathbf{C_{26}H_{23}N_6O_3^+}$: 489.1651 $[M-H+Na]^+$; found 489.1664 $[M-H+Na]^+$.

Compound D:

^{1}H NMR (600 MHz, MeOD) δ 8.35 / ppm (H-guanidino, d, J = 9.2 Hz, 1H), 8.16 (H-guanidino, d, J = 7.6 Hz, 2H), 8.11 (H-guanidino, t, J = 8.6 Hz, 2H), 8.02 (H-guanidino, d, J = 1.4 Hz, 2H), 7.97 (H-guanidino, t, J = 7.6 Hz, 1H), 7.91 (H-guanidino, d, J = 7.8 Hz, 1H), 7.11 (H-PBA, d, J = 4.2 Hz, 1H), 6.98 (H-PBA, d, J = 4.1 Hz, 1H), 4.64 (α, Lys, t, J = 7.9 Hz, 1H), 3.45 – 3.39 (CH_2-3, PBA, m, 2H), 2.94 (ε, Lys, t, J = 7.5 Hz, 2H), 2.44 (CH_2-1,

PBA, t, J = 13.2 Hz, 2H), 2.19 (CH_2-2, PBA, t, J = 15.1 Hz, 2H), 2.02 (β, Lys, t, J = 15.5 Hz, 1H), 1.88 (β', Lys, t, J = 15.2 Hz, 1H), 1.75 - 1.71 (δ, Lys, m, 2H), 1.60 - 1.56 (γ, Lys, m, 2H).

^{13}C NMR (151 MHz, MeOD) δ / ppm 173.5 (CO), 171.6 (CO), 160.4 (CO), 160.0 (CO), 155.9 (CNH), 135.9 (C, PBA), 131.8 131.4 (C, guanidino), 130.9, 130.0 (C, PBA), 128.6, 127.1 (CH, guanidino), 126.9, 126.3, 125.8, 125.6, 124.8, 124.7, 124.5, 124.4 (CH, PBA), 123.1, 117.1, 114.7, 112.5 (C, PBA), 51.8 (α, Lys), 39.1 (ε, Lys), 33.0 (CH_2-1, PBA), 32.2 (CH_2-3, PBA), 31.0 (β, Lys), 27.2 (δ, Lys), 26.7 (CH_2-2, PBA), 22.2 (γ, Lys).

HRMS (MALDI-TOF/TOF) m/z = calc. for $\mathbf{C_{33}H_{38}N_8O_4}^{2+}$: 609.2938 $[M-H]^+$; found 609.2960 $[M-H]^+$.

Compound E:

^{1}H NMR (300 MHz, DMSO) δ / ppm 12.44 (NH, guanidino, s, 1H), 12.00 (NH, s, 1H), 9.99 (NH, hyd, s, 1H), 9.85 (NH, hyd, s, 1H), 8.85 (NH, amide, s, 1H), 8.62 (NH_2, PGA, bs, 2H), 8.46 (NH_2, PGA, bs, 2H), 8.39 (d, J = 9.3 Hz, 7H), 8.30 – 8.16 (m, 21H), 8.12 (dd, J = 4.1, 3.1 Hz, 9H), 8.05 (dd, J = 14.2, 6.6 Hz, 7H), 7.96 (dd, J = 7.7, 4.4 Hz, 6H), 7.53 (CH, PGA, s, 1H), 6.89 (CH, PGA, s, 1H), 3.97 (α, Gly, s, 2H), 3.38 – 3.29 (CH_2-3, PBA, m, 2H), 2.35 - 2.32 (CH_2-1, PBA, m, 11H), 2.10 - 2.02 (CH_2-2, PBA, m, 2H).

^{13}C NMR (151 MHz, DMSO) δ / ppm 170.9 (CO), 167.8 (CO), 159.6 (CO), 159.4 (CO), 155.4 (CNH), 136.5, 132.5 (C, guanidino), 130.9, 130.4 (CH, guanidino), 129.3 (C, PBA), 128.2, 127.6, 127.5, 127.3 (CH, PCA), 127.3, 126.5, 126.1, 125.6, 124.9 (C, PBA), 124.9, 124.8, 124.2, 124.1, 123.6 (CH, PBA), 45.5 (α, Gly), 32.9 (CH_2-1, PBA), 32.1 (CH_2-3, PBA), 27.6 (CH_2-2, PBA).

HRMS (MALDI-TOF/TOF) m/z = calc. for $\mathbf{C_{29}H_{28}N_7O_4}^+$: 538.2203 $[M]^+$; found 538.2197 $[M]^+$.

Compound F:

^{1}H NMR (300 MHz, DMSO) δ / ppm 12.54 (NH, guanidino, s, 1H), 12.20 (NH, s, 1H), 8.91 (NH, amide, d, J = 6.0 Hz, 1H), 8.74 (NH_2, PGA, bs, 2H), 8.58 (NH_2, PGA, bs, 2H), 8.48 - 7.90 (CH, PMA, NH_3^+, Lys, m, 17H), 7.62 (CH, PGA, s, 1H), 6.92 (CH, PGA, s, 1H), 5.03

(CH_2, PMA, d, J = 5.2 Hz, 2H), 4.52 (α, Lys, d, J = 4.8 Hz, 1H), 2.70 (ε, Lys, s, 2H), 1.76 (β, Lys, d, J = 5.8 Hz, 2H), 1.63 – 1.41 (δ, γ, Lys, m, 4H).

^{13}C NMR (75 MHz, DMSO) δ / ppm 171.5 (CO), 159.7 (CO), 158.9 (CO), 155.6 (CNH), 132.7, 132.5 (C, PGA), 130.7, 130.3 (CH, PGA), 130.0 (C, PMA), 128.3, 127.9, 127.4, 127.3, 126.9, 126.4 (CH, PMA), 126.2, 125.5, 125.1 (C, PMA), 124.7, 123.9, 123.9 (CH, PMA), 123.1, 115.8, 113.6 (C, PMA), 52.9 (α, Lys), 38.4 (CH_2, PMA), 31.4 (ε, Lys), 30.5 (β, Lys), 26.5 (δ, Lys), 22.6 (γ, Lys).

HRMS (MALDI-TOF/TOF) m/z = calc. for $\mathbf{C_{30}H_{33}N_7O_3^{2+}}$: 538,2567 $[M-H]^+$; found 538,2580 $[M-H]^+$.

Compound CIA:

^{1}H NMR (600 MHz, DMSO) δ 12.47 (s, 1H, NH), 10.93 (s, 1H, NH), 8.84 (dd, J = 18.6, 7.6 Hz, 1H, Ar), 8.75 (d, J = 8.7 Hz, 1H, Ar), 8.71 (d, J = 7.2 Hz, 1H, Ar), 8.25 – 8.09 (m, 5H, Ar + NH), 8.07 – 8.01 (m, 2H, Ar), 7.95 (dd, J = 26.2, 17.8 Hz, 2H, Ar), 7.85 – 7.81 (m, 1H, Ar), 7.55 (dd, J = 8.3, 1.6 Hz, 1H, Ar), 7.43 (d, J = 7.0 Hz, 1H, Ar), 6.99 (dd, J = 4.0, 2.4 Hz, 1H, Ar), 6.87 (s, 1H, CH), 4.67 (dd, J = 15.1, 7.0 Hz, 1H, CH), 4.56 – 4.50 (m, 1H, CH), 4.43 (t, J = 6.7 Hz, 1H, CH), 4.23 (s, 3H, CH_3), 3.59 (s, 3H, CH_3), 3.18 – 3.01 (m, 2H, CH_2), 2.10 – 1.97 (m, 2H, CH_2), 1.87 – 1.63 (m, 4H, 2X CH_2) ppm.

^{13}C NMR (151 MHz, DMSO) δ 159.37, 155.94, 149.79, 145.88, 141.95, 138.51, 133.89, 132.17, 127.78, 127.32, 126.19, 124.88, 124.70, 123.59, 123.40, 121.74, 118.80, 115.68, 115.56, 109.25, 88.21, 67.21, 53.66, 52.90, 49.31, 46.43, 43.18, 27.69 ppm.

HRMS (MALDI-TOF/TOF) m/z calcd for $C_{35}H_{37}BrN_{10}O_4S^{2+}$ ($[M-H]^+$) 771,1825, found 771,1835.

Molecular modelling

Model setup

The semi-closed conformation of hDPP III and its inactive E451A mutant obtained in our earlier studies were used to build the complexes with compounds **A**, **D**, **E**, **F** and **CIA**, since it was shown that hDPP III preferably adopt such a form in water (Tomić, Gonzalez & Tomić 2012; Tomić, Berynskyy, Wade & Tomić 2015). Importance of the amino acid residues and

ligands protonation states have been discussed by many authors (see for example Borštnar et al 2012). Protonation of the amino acid residues and ligands used in this study was assigned in a way to fulfilled experimental conditions and the reaction mechanism requirements (Tomić et al. 2016). All Arg and Lys residues were positively charged and all Glu and Asp residues were negatively charged. Protonation states of histidine residues were determined with respect to their local environment, i.e. their role in the zinc ion coordination and their ability to form hydrogen bonds with neighbouring amino acid residues. His568 was positively charged according to the results of our earlier performed study of the human DPP III reaction mechanism (Tomić et al. 2016). AM1-BCC charges were assigned to ligands taking care of the charged groups (Scheme 1).

The 3D structures of ligands were constructed using the program GaussView 5.0. The ligand docking was performed by the program AutoDock (AutoDock 4.2.6, (Morris et al. 2009)). Center of the docking box was placed on the Zn^{2+}, and its size was 80 × 80 × 80 $Å^3$ while the grid spacing was 0.25 Å. Ligands were considered flexible and the docking was performed by Lamarckian Genetic Algorithm (LGA) using default parameters. The complexes were parametrized by the AMBERTools16 modules antechamber and tleap using GAFF (Wang, Wolf, Caldwell, Kollman & Case 2004) and ff14SB (Maier et al. 2015) force fields to parameterize the substrate and the protein, respectively. For the zinc cation, the hybrid bonded-nonbonded parameters developed by us were used (Tomić et al. 2019). Tomić et al. 2019). (REF New Zinc Ion Parameters Suitable for Classical MD Simulations of Zinc Metallopeptidases Authors: Antonija Tomić, Gordan Horvat, Michael Ramek, Dejan Agić, Hrvoje Brkic, Sanja Tomić (DOI: 10.1021/acs.jcim.9b00235

The complexes were solvated in an octahedron box filled with TIP3P water molecules ensuring an 11 Å thick water molecules buffer around the protein. Na^+ ions were added to neutralize the system and were placed in the vicinity of the charged amino acid residues at the protein surface.

Molecular dynamics simulations

The solvated complexes were geometry optimized and simulated for at least 100 ns. The protein geometry was optimized in 3 cycles with different restraints. During the first cycle, 1500 optimization steps were performed, where the first 450 steps were of the steepest descent method, and the rest was the conjugate gradient. Both, the protein atoms and the

metal ion, were constrained using a harmonic potential of 32 kcal/(molÅ^2), in order to equilibrate water molecules. In the second cycle, 2500 steps, the metal ion, and the protein backbone were constrained with 12 kcal/(mol Å^2). During the third cycle (9500 steps) no constraints were applied. The minimized system was heated from 0 to 300 K during 30 ps using a canonical ensemble (NVT), followed equilibration stage of 70 ps during which the water density was adjusted and at least 100 ns of the productive molecular dynamics (MD) simulations (NPT conditions). Constant temperature (300 K) and pressure (1 atm) were ensured using Langevin dynamics with a collision frequency of 1 ps^{-1}, and Berendsen barostat, respectively. In the case of CIA-M3 complex, after 100 ns of the productive MD simulations the system was in two periods (from 100 ns - 130 ns and from 190 ns – 220 ns) simulated at decreased temperature (100 K). The time step during the periods of heating and the water density adjustment was 1 fs, and for the rest of the simulation 2 fs (to restrain the motion of hydrogens the SHAKE algorithm was used). The periodic boundary conditions were utilized wherein the electrostatic interactions were calculated using the particle-mesh Ewald method. The simulations were performed by the pmemd module from the AMBER16 package running at GPU.

Data analysis

In order to analyse and to characterize the stability of the complexes during MD simulations, RMSD of the protein backbone atoms as well as of the ligand heavy (all atoms except hydrogens) were calculated. According to our earlier studies radius of gyration (Rg) is used as an estimate of the protein compactness, while the ligand impact to the local protein dynamics was estimated from the RMSF analysis. Detail insight into the protein-ligand interaction was obtained from the intermolecular interactions analysis. All these analyses were performed within the CPPTRAJ module of the AmberTools16 program package. The hydrogen bond (bond and angle cut-off values of 3.0 Å and 135°, respectively, were used to define HB) population was calculated as the ratio of the number of generated frames containing the bond and the total number of frames (Hbpop= N(frameswith Hbond)/N(frames total)). In a case when a residue forms multiple hydrogen bonds, the hydrogen bond population is expressed as a sum of these values. Interactions present in <2% of generated structures were omitted.

The MM-PBSA energies were calculated at the final 5 ns of the productive MD simulations

using the MMPBSA.py script available within the Amber16 suite. Since both the enzyme active site and ligands are charged, the nonlinear Poisson–Boltzmann solver was used in conjunction with the P3M method for computing the electrostatic energy components. The cut-off distance for van der Waals interactions was set to 11 Å. Internal and external dielectric constants were set at 2.0 and 80.0, respectively. The salt concentration was 0.10 M.

Acknowledgements

The work has been supported by Croatian Science Foundation projects: IP-2018-01-2936 and IP-2018-01-5475. We thank Peter Macheroux team (TU-Graz, Austria) for valuable support and discussions and Marko Tomin for his help with AutoDock program.

References:

Abramić, M., Šimaga, S., Osmak, M., Cicin-Sain, L., Vukelic, B., Vlahoviček, K. & Dolovčak, L. (2004). Highly reactive cysteine residues are part of the substrate binding site of mammalian dipeptidyl peptidases III. *International Journal of Biochemistry & Cell Biology 36*: 434-446.

Agić, D., Brkić, H., Tomić, S., Karačić, Z., Špoljarević, M., Lisjak, M., Beslo, D. & Abramić, M. (2017). Validation of flavonoids as potential dipeptidyl peptidase III inhibitors: Experimental and computational approach. *Chemical Biology & Drug Design 89*: 619-627.

Armitage, B. A. (2005). DNA Binders and Related Subjects: Cyanine dye-DNA interactions: Intercalation, groove binding, and aggregation. *Topics in Current Chemistry 253*: 55-76.

Baršun, M., Jajčanin, N., Vukelić, B., Špoljarić, J. & Abramić, M. (2007). Human dipeptidyl peptidase III acts as a post-proline-cleaving enzyme on endomorphins. *Biological Chemistry 388*: 343-348.

Borštnar, R., Repič, M., Lynn Kamerlin, S. C., Vianello, R., Mavri, J. (2012). Computational Study of the pKa Values of Potential Catalytic Residues in the Active Site of Monoamine Oxidase B. *Journal of Chemical Theory and Computation 8*: 3864–3870.

Dhanda, S., Singh, H., Singh, J. & Singh, T. P. (2008). Functional characterization and specific effects of various peptides on enzymatic activity of a DPP-III homologue from goat brain. *Journal of Enzyme Inhibition and Medicinal Chemistry 23*: 174-181.

GraphPad GraphPad Software. San Diego California USA, GraphPad.

Korshun, V. A., Stetsenko, D. A. & Gait, M. J. (2002). Novel uridin-2′-yl carbamates: synthesis, incorporation into oligodeoxyribonucleotides, and remarkable fluorescence properties of 2′-pyren-1-ylmethylcarbamate. *Journal of the Chemical Society, Perkin Transactions 1*: 1092-1104.

Kostenko, E., Dobrikov, M., Pyshnyi, D., Petyuk, V., Komarova, N., Vlassov, V. & Zenkova, M. (2001). 5'-bis-pyrenylated oligonucleotides displaying excimer fluorescence provide sensitive probes of RNA sequence and structure. *Nucleic Acids Res 29*: 3611-3620.

Kumar, P., Reithofer, V., Reisinger, M., Wallner, S., Pavkov-Keller, T., Macheroux, P. & Gruber, K. (2016). Substrate complexes of human dipeptidyl peptidase III reveal the mechanism of enzyme inhibition. *Scientific Reports 6*.

Lakowicz, J. R. (1999). *Principles of Fluorescence Spectroscopy*. New York, Kluwer Academic/Plenum.

Lehrer, S. S. (1997). Intramolecular pyrene excimer fluorescence: A probe of proximity and protein conformational change. *Fluorescence Spectroscopy 278*: 286-295.

Mačak Safranko, Z., Sobočanec, S., Šarić, A., Jajčanin-Jozić, N., Krsnik, Z., Aralica, G., Balog, T. & Abramić, M. (2015). The effect of 17 beta-estradiol on the expression of dipeptidyl peptidase III and heme oxygenase 1 in liver of CBA/H mice. *Journal of Endocrinological Investigation 38*: 471-479.

Mahara, A., Iwase, R., Sakamoto, T., Yamana, K., Yamaoka, T. & Murakami, A. (2002). Bispyrene-conjugated 2 '-O-methyloligonucleotide as a highly specific RNA-recognition probe. *Angewandte Chemie-International Edition 41*: 3648-3650.

Maier, J. A., Martinez, C., Kasavajhala, K., Wickstrom, L., Hauser, K. E. & Simmerling, C. (2015). ff14SB: Improving the Accuracy of Protein Side Chain and Backbone Parameters from ff99SB. *J Chem Theory Comput 11*: 3696-3713.

Matić, J., Šupljika, F., Tir, N., Piotrowski, P., Schmuck, C., Abramić, M., Piantanida, I. & Tomić, S. (2016). Guanidiniocarbonyl-pyrrole-aryl conjugates as inhibitors of human dipeptidyl peptidase III: combined experimental and computational study. *Rsc Advances 6*: 83044-83052.

Matovina, M., Agić, D., Abramić, M., Matić, S., Karačić, Z. & Tomić, S. (2017). New findings about human dipeptidyl peptidase III based on mutations found in cancer. *Rsc Advances 7*: 36326-36334.

Morris, G. M., Huey, R., Lindstrom, W., Sanner, M. F., Belew, R. K., Goodsell, D. S. & Olson, A. J. (2009). AutoDock4 and AutoDockTools4: Automated Docking with Selective Receptor Flexibility. *Journal of Computational Chemistry 30*: 2785-2791.

Mycek, M-A. and Pogue, B. W. (2003) Handbook of Biomedical Fluorescence, CRC Press, Boca Raton, USA.

Pang, X. L., Shimizu, A., Kurita, S., Zankov, D. P., Takeuchi, K., Yasuda-Yamahara, M., Kume, S., Ishida, T. & Ogita, H. (2016). Novel Therapeutic Role for Dipeptidyl Peptidase III in the Treatment of Hypertension. *Hypertension 68*: 630-641.

Prajapati, S. C. & Chauhan, S. S. (2011). Dipeptidyl peptidase III: a multifaceted oligopeptide N-end cutter. *Febs Journal 278*: 3256-3276.

Prajapati, S. C. & Chauhan, S. S. (2016). Human dipeptidyl peptidase III mRNA variant I and II are expressed concurrently in multiple tumor derived cell lines and translated at comparable efficiency in vitro. *Molecular Biology Reports 43*: 457-462.

Schmuck, C. (2011). A Journey through 12 Years of Interacting Molecules: From Artificial Amino Acid Receptors to the Recognition of Biomolecules and Switchable Nanomaterials. *Synlett*: 1798-1815.

Shi, C. H., Wu, J. B. & Pan, D. F. (2016). Review on near-infrared heptamethine cyanine dyes as theranostic agents for tumor imaging, targeting, and photodynamic therapy. *Journal of Biomedical Optics 21*.

Šmidlehner, T., Karačić, Z., Tomić, S., Schmuck, C. & Piantanida, I. (2018). Fluorescent cyanine-guanidiniocarbonyl-pyrrole conjugate with pH-dependent DNA/RNA recognition and DPP III fluorescent labelling and inhibition properties. *Monatshefte Fur Chemie 149*: 1307-1313.

Špoljarić, J., Salopek-Sondi, B., Makarević, J., Vukelić, B., Agić, D., Šimaga, S., Jajčanin-Jozić, N. & Abramić, M. (2009). Absolutely conserved tryptophan in M49 family of

peptidases contributes to catalysis and binding of competitive inhibitors. *Bioorganic Chemistry 37*: 70-76.

Tatikolov, A. (2012). Polymethine dyes as spectral-fluorescent probes for biomacromolecules. *Journal of Photochemistry and Photobiology C: Photochemistry Reviews 13*: 55 -90.

Tomić, A., Berynskyy, M., Wade, R. C. & Tomić, S. (2015). Molecular simulations reveal that the long range fluctuations of human DPP III change upon ligand binding. *Molecular Biosystems 11*: 3068-3080.

Tomić, A., Gonzalez, M. & Tomić, S. (2012). The Large Scale Conformational Change of the Human DPP III-Substrate Prefers the "Closed" Form. *Journal of Chemical Information and Modeling 52*: 1583-1594.

Tomić, A., Kovačević, B. & Tomić, S. (2016). Concerted nitrogen inversion and hydrogen bonding to Glu451 are responsible for protein-controlled suppression of the reverse reaction in human DPP III. *Physical Chemistry Chemical Physics 18*: 27245-27256.

Wang, J., Wolf, R. M., Caldwell, J. W., Kollman, P. A. & Case, D. A. (2004). Development and testing of a general amber force field. *Journal of Computational Chemistry 25*: 1157-1174.

Wang, E., Sun, H., Wang, J., Wang, Z., Liu, H., Zhang, J.Z.H., Hou, T. (2019) End-Point Binding Free Energy Calculation with MM/PBSA and MM/GBSA: Strategies and Applications in Drug Design.*Chemical Reviews*. 10.1021/acs.chemrev.9b00055.

Winnik, F. M. (1993). Photophysics of Preassociated Pyrenes in Aqueous Polymer-Solutions and in Other Organized Media. *Chemical Reviews 93*: 587-614.

Yamamoto, Y., Hashimoto, J., Shimamura, M., Yamaguchi, T. & Hazato, T. (2000). Characterization of tynorphin, a potent endogenous inhibitor of dipeptidyl peptidaseIII. *Peptides 21*: 503-508.

Yamana, K., Zako, H., Asazuma, K., Iwase, R., Nakano, H. & Murakami, A. (2001). Fluorescence detection of specific RNA sequences using 2'-pyrene-modified oligoribonucleotides. *Angewandte Chemie-International Edition 40*: 1104-1106.